Journal of Electrical and Computer Engineering Innovations
(JECEI)
Journal homepage: http://www.jecei.sru.ac.ir

SRTTU JECEI

Research paper

Design of Miniaturized Microstrip Antenna with Semi-Fractal Structure For GPS/GLONASS/Galileo Applications

S. Komeylian[1], M. Tayarani[1,*], S. H. Sedighy[2]

[1]*Department of Electrical Engineering, Iran University of Science and Technology, Tehran 1684613114, Iran.*

[2]*School of New Technologies, Iran University of Science and Technology, Tehran 16846-13114, Iran.*

Article Info

Article History:
Received 08 November 2022
Reviewed 24 December 2022
Revised 08 February 2023
Accepted 01 March 2023

Keywords:
Miniaturized antenna
Low-profile antenna
Semi-fractal structure
Multiple feed configuration
Pure polarization
RHCP antenna

*Corresponding Author's Email Address:
m_tayarani@iust.ac.ir

Abstract

Background and Objectives: Microstrip patch antennas are widely used due to their advantages of compact size and easy fabrication compared to other types. However, they have low-performance parameters. As a result, several techniques are used to improve performance parameters in newly designed microstrip antennas. In this study, a novel miniaturized microstrip antenna with circular polarization (CP) is proposed for GNSS applications.

Methods: In the design process, the semi-fractal structure is used to reduce the antenna size. Circular polarization is generated using a three-feed configuration with 120° phase shift. The CP value is increased by use of perturbing slots and also removing the corners. The novel design of the feeding network and also considering the ground size same as the patch layer, keep the antenna size small. The co-axial probe is used in the feeding network and it is printed on Taconic RF-43 substrate with a low loss tangent of 0.0033. Numerical simulation is applied via CST commercial software to evaluate the antenna performance. The simulations are repeated in two other software, HFSS and FEKO, to validate the study.

Results: The proposed antenna has a compact size of 17.56 cm^2. The single-layer structure of the designed antenna leads to easy fabrication feature. The proposed antenna has a bandwidth of 55 MHz (1.558-1.614 GHz). It can operate at GPS L1 (1575 MHz), GLONASS G1 (1602 MHz), Galileo E1 (1589 MHz), and E2 (1561 MHz) bands. Results show a high front-to-back ratio (FBR) of 40 *dB*, RHCP gain of 3.45 *dB*, and pure CP with axial ratio (AR) beamwidth of 108°. Furthermore, the phase center variation (PCV) is less than 0.16 *mm.*

Conclusion: Key features of the proposed antenna are its novel fractal structure that leads to compact size, high front-to-back ratio, wide RHCP beamwidth with desirable bandwidth, and axial ratio beamwidth.

Introduction

Microstrip antennas with circular polarization are widely used in satellite applications [1]–[8], such as global positioning systems (GPS) and global navigation satellite systems (GLONASS) to reduce multipath reflection effects. A circularly polarized radiated field is generally generated by the excitation of two orthogonal modes with a 90° phase difference[9], [10]. In the single feed configuration, the feed should be located at a convenient position to excite orthogonal modes and produce CP [5], [11], [20], [21], [12]–[19].

Orthogonal modes are generated by perturbing antenna structure, such as creating narrow slits near the edges of the patch [22], arc-shaped or orthogonality-located slots [14], [23], and also truncated corners of the patch [1]. Multiple feed patch antennas provide a larger CP purity and higher performance [1], but they generally have a larger size for feeding networks [24]. In most satellite applications, the size of the antenna is important [21], [25].

Fractal geometry is a low-cost method for miniaturizing the microstrip patch antenna which is used in several studies [26], [27]. Fractals are geometric shapes composed of multiple iterations of a single shape [6], which allows for a reduction in metallization and resonant frequency [28].

In this study, a novel design of a microstrip antenna with semi-fractal geometry is presented. The proposed antenna operates at GPS L1 (1575 MHz), GLONASS G1 (1602 MHz), Galileo E1 (1589 MHz), and E2 (1561 MHz) bands. The antenna is compact, low-profile, and planar. Details of the design process and simulation results are presented and discussed in the following sections.

Antenna Design

The proposed microstrip antenna consists of a patch layer, a Taconic RF-43 substrate, a ground plane, a feeding substrate, and a feeding network. To miniaturize the antenna with a low-cost method, a semi-fractal structure is employed. Then optimization is done to obtain the best geometry with the best performance.

The fractal structure, design process, and feeding techniques used in this study, are described as follows.

A. Fractal Structure

In the first step of producing the patch geometry, an equilateral triangle, as the first polygon, is selected. The main triangle size is obtained by optimization. The smallest triangle is selected which satisfies design constraints containing operating frequency and desirable bandwidth. The main triangle has a side length of 57 mm. In general, patch antenna has low bandwidth. It is proved that by removing the corners of the patch geometry, the bandwidth will be increased [29]. As a result, in the next step, the corners of the main triangle are removed.

Fig. 1 shows the current distribution on the surface of arced vertex triangle at f=1.52 GHz, the resonant frequency of the first step geometry. As is clear, more current is concentrated on the patch boundaries. So, by increasing the boundaries of the antenna geometry, the current will be increased and as a result, more radiation is achieved. For this reason, a semi-fractal structure is selected to develop the patch geometry.

The fractal part size at each step is chosen via optimization with the aim of the smallest patch satisfying the constraints, the same as the main triangle.

The fractal generation is started by removing the scaled, reversed shape triangle from the center of the patch as illustrated in Fig. 2-a. In the next step, again a scaled, reversed triangle is truncated from the center of the patch as shown in Fig. 2-b. By repeating the previous steps with a scaled triangle, the geometry will be as Fig. 2-c. The final shape is obtained by removing two triangles from the external edges of the central triangle, which is illustrated in Fig. 2-d.

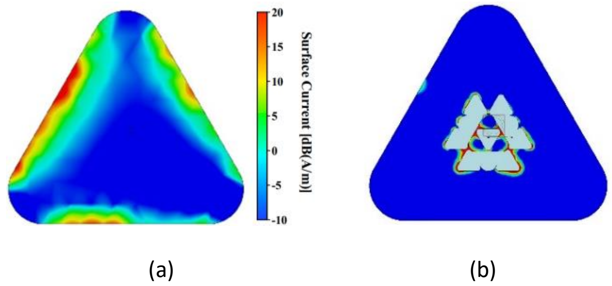

Fig. 1: Current distribution on the patch geometry (a) Before fractal generation, (b) After fractal generation.

The effects of each step geometry generation are evaluated in terms of return loss (S_{11}). As shown in Fig. 3, by each iteration, the resonant frequency is decreased, hence compression occurs. The compression ratio at the end of fractal structure generation is 12%.

As illustrated in Fig. 4, the edges of the designed patch structure, are removed by contraction of the reversed main triangle from the patch geometry. Converting the triangle shape to the hexagon, increases the antenna bandwidth, as shown in Fig. 5. In general, it can be concluded that tending the patch geometry to a circle shape will increase the antenna bandwidth.

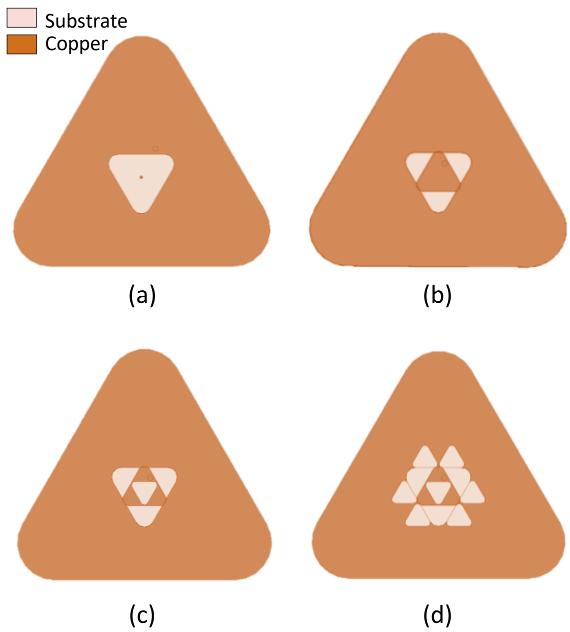

Fig. 2: The fractal structure generation steps from (a) to (d).

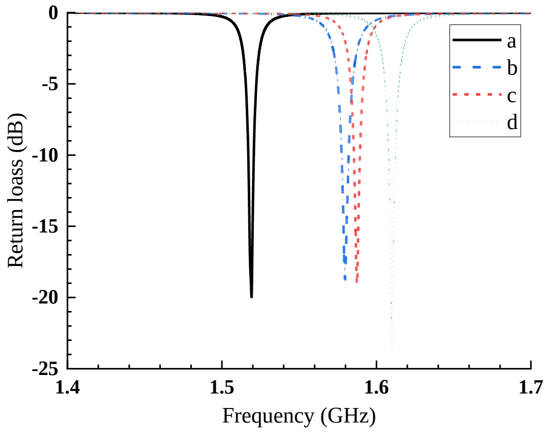

Fig. 3: Effects of fractal iterations.

B. Design Process

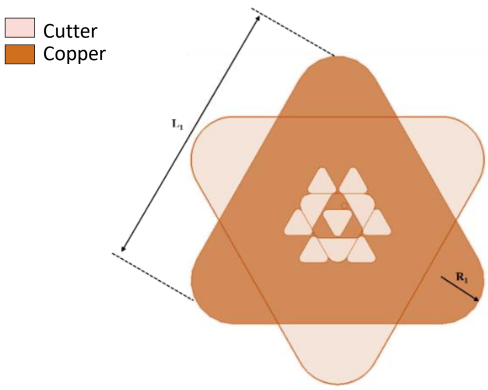

Fig. 4. Truncating edges of the designed antenna.

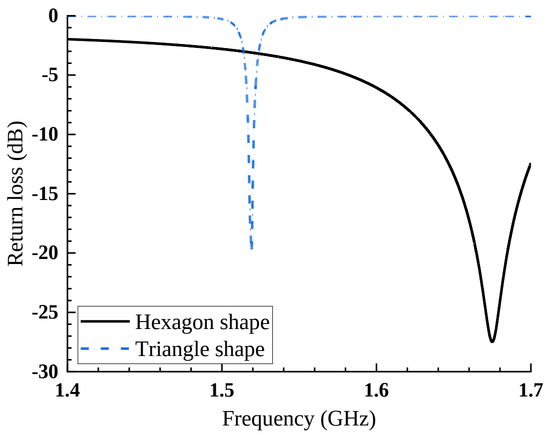

Fig. 5: Effect of converting the triangle to the hexagon.

The final geometry of the proposed microstrip antenna is shown in Fig. 6. The geometric parameters of the designed antenna and their optimum values are presented in Table 1.

As is clear, a hexagon slot and three circular slots are printed on the patch, which improve the antenna resonant frequency adjustment as illustrated in Fig. 7.

Table 1: The geometric parameters

Geometric parameters	Optimum value (mm)	Geometric parameters	Optimum value (mm)
L_1	39.55	R_1	14.14
L_2	26	R_2	1.24
L_3	22	R_3	1.8
L_4	10.2	R_f	3
L_5	6.79	t_1	0.16
L_6	3.99	t_2	0.2
L_7	3.38	ϕ_1	1.12
L_h	12.8	h	3

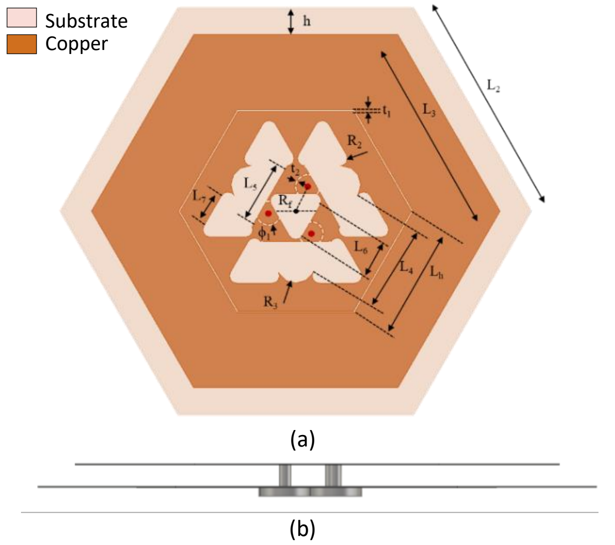

Fig. 6: The final geometry of the designed antenna; (a) Front view, (b) Side view.

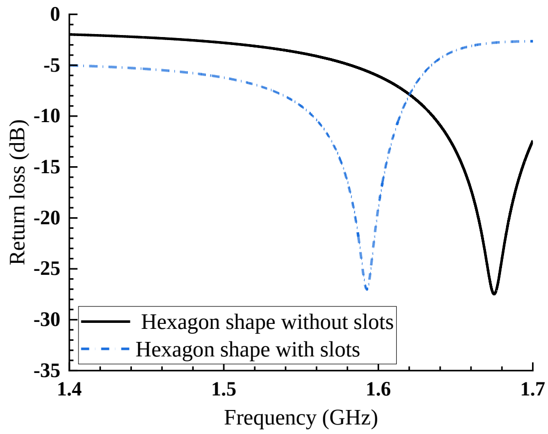

Fig. 7: The effect of adding slots.

The total compression ratio at the end of geometry design (hexagon shape with slots) is 30% with an increase of bandwidth. The hexagon patch layer is etched onto the upper side of the Taconic RF-43 substrate with relative permittivity of 4.3 and a loss tangent of 0.0033, and the feeding structure is printed on the other side. The substrate dimensions are 50mm×50mm×2mm, and the patch has a compact size of 40mm×40mm.

C. Parametric Study

The effects of key geometric parameters on the proposed antenna performance are analyzed and discussed. The parameters consist of the main triangle lateral length (L_1), the fractal triangle vertex arc radius (R_2), and the hexagon slot length (L_h). Sensitivity to the material has been checked by evaluating the variable relative permittivity (ε_r), between 4.1 and 4.5. The thickness of the substrate (t_{sub}) is also studied. Except for the studied parameter, other parameters have been constant.

The effect of the main triangle lateral length (L_1) on the proposed antenna bandwidth is depicted in Fig. 8.

As clearly shown, the optimum value of L_1=39.55 mm will result in operating at desirable frequency bands. The reduced L_1 does not satisfy below -10 dB return loss and increased L_1 shifts the operating range to lower frequencies.

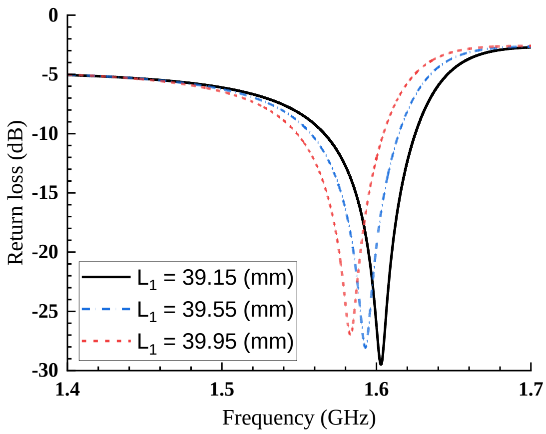

Fig. 8: The effect of the main triangle lateral length.

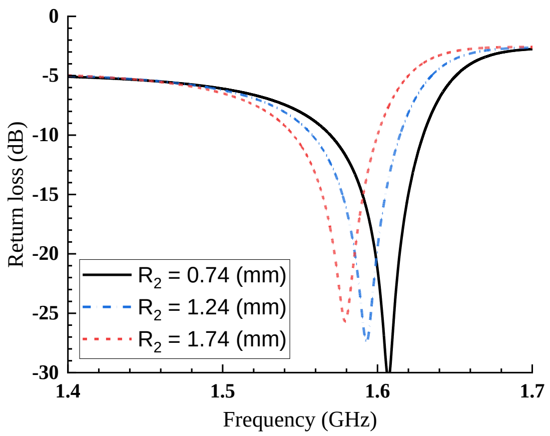

Fig. 9: The impact of the vertex arc radius.

Fig. 9 shows the impact of the vertex arc radius (R_2). The effect of R_2 parameter is the same as L_1, and it has the optimum value of R_2 =1.24 mm.

The hexagon slot length (L_h) effect on the performance of the proposed antenna is illustrated in Fig. 10. It is shown that by increasing L_h, the -10 dB return loss bandwidth is improved and the operation bands will shift to high frequencies. The desirable performance is achieved at $L_{h=}$ 12.8 mm.

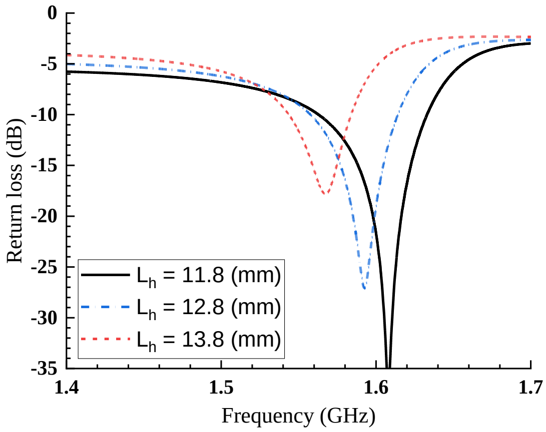

Fig. 10: The effect of hexagon slot length.

The substrate material sensitivity is studied by evaluating the effect of relative permittivity on return loss. Fig. 11 shows that an increase or decrease of ε_r, considerably changes the operating frequency range.

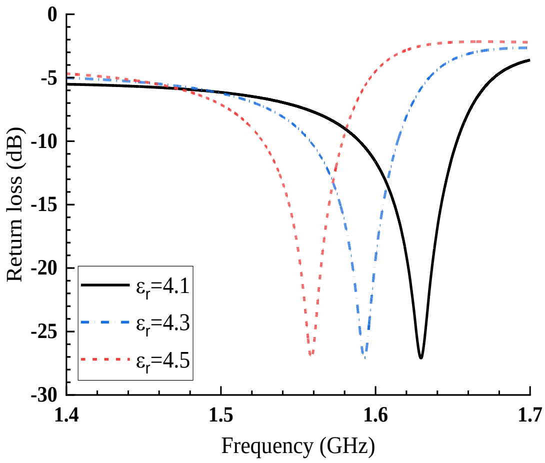

Fig. 11: The effect of substrate relative permittivity.

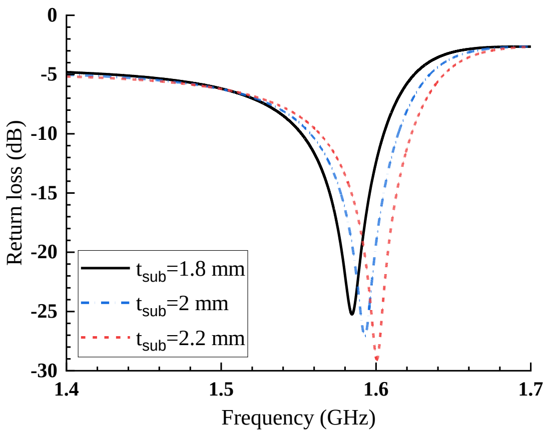

Fig. 12: The effect of substrate thickness.

Fig. 12 demonstrates the effect of substrate thickness. Decreasing t_{sub} shifts the resonant frequency to a lower value and an increase in it shifts to the higher value of resonant frequency. The optimum value of t_{sub}= 2 mm leads to operating at the desired frequency range.

D. Feeding Techniques

In this study, a three-feed configuration is designed as shown in Fig. 13. The feeding network is designed with a coaxial probe to be single layer and low-profile. Theoretical analysis is done to find the required temporal phase shift for CP. The electric field created by feeding port 1 on the Z-axis is called E_1:

$$E_1 = \begin{bmatrix} e_{0x} \\ e_{0y} \\ e_{0z} \end{bmatrix} \tag{1}$$

The field created by the second feeding port is called E_2. Considering the symmetric feeding configuration, the electric field resulting from E_2 is similar to E_1, with the difference in spatial phase shift $\theta = \frac{2\pi}{3}$:

$$E_2 = e^{-\varphi j}\left[T\left(\frac{2\pi}{3}\right)\right]\begin{bmatrix} e_{0x} \\ e_{0y} \\ e_{0z} \end{bmatrix} \tag{2}$$

The T matrix represents the rotation of θ around the Z-axis. Also, the time delay between the excitation of the second port and the first port is considered as φ.

$$[T(\theta)] = \begin{bmatrix} \cos\theta & -\sin\theta & 0 \\ \sin\theta & \cos\theta & 0 \\ 0 & 0 & 1 \end{bmatrix} \tag{3}$$

Similarly, the electric field caused by the third feeding port is calculated as equation (4).

$$E_3 = e^{-2\varphi j}\left[T\left(\frac{4\pi}{3}\right)\right]\begin{bmatrix} e_{0x} \\ e_{0y} \\ e_{0z} \end{bmatrix} \tag{4}$$

Hence:

$$E_{total} = \left(1 + e^{-j\varphi}\left[T\left(\frac{2\pi}{3}\right)\right] + e^{-2j\varphi}\left[T\left(\frac{4\pi}{3}\right)\right]\right)\begin{bmatrix} e_{0x} \\ e_{0y} \\ e_{0z} \end{bmatrix} \tag{5}$$

E_{total} is simplified to equation (6).

$$E_{total} = \frac{1}{2}\begin{bmatrix} ue_{0x} - ve_{0y} \\ ve_{0x} + ue_{0y} \\ 2\frac{1-e^{-3j\varphi}}{1-e^{-j\varphi}}e_{0z} \end{bmatrix} = \begin{bmatrix} e_x \\ e_y \\ e_z \end{bmatrix} \tag{6}$$

where u and v are defined as (7) and (8).

$$u = (1 + e^{j\alpha} + e^{2j\alpha}) + (1 + e^{j\beta} + e^{2j\beta}) \tag{7}$$

$$v = -j(1 + e^{j\alpha} + e^{2j\alpha}) + j(1 + e^{j\beta} + e^{2j\beta}) \tag{8}$$

Also, β is implied as (9).

$$\beta = -\varphi - \frac{2\pi}{3} \tag{9}$$

And α is defined as (10).

$$\alpha = -\varphi + \frac{2\pi}{3} \tag{10}$$

Therefore, the right-handed electric field is calculated from (11).

$$|R| = \left|\frac{e_x - je_y}{2}\right| = \left|(1 + e^{j\beta} + e^{2j\beta})\right|\left|(e_{0x} - je_{0y})\right| \tag{11}$$

Similarly, the left-handed electric field is obtained from (12).

$$|L| = \left|\frac{e_x + je_y}{2}\right| = \left|(1 + e^{j\alpha} + e^{2j\alpha})\right|\left|(e_{0x} + je_{0y})\right| \tag{12}$$

As shown in equation (11), β=0 leads to maximum R and thus pure right-handed circular polarization (RHCP). So according to equation (9) pure CP is achieved by setting the temporal and spatial phase shifts with the same value and negative sign. In this study the temporal phase shift for symmetric three-feed configuration is $-\frac{2\pi}{3}$. By setting $\phi = -\frac{2\pi}{3}$ and $\alpha = \frac{4\pi}{3}$ the left-handed electric field shown in (12) will be zero.

The feeding network consists of transmission lines and a 3-way power divider. A Schematic of the feeding network elements is shown in Fig. 14. The length difference of the transmission lines, leads to the 120° phase difference between the ports. The power divider used in this study has a novel design. It consists of two lumped resistors of 75Ω for isolation and also some open-circuited lines for matching. The final design of the feeding network is simulated in ADS. The designed feeding network is fabricated on a Taconic RF-43 substrate with 0.508 mm thickness and a dielectric constant of 4.3.

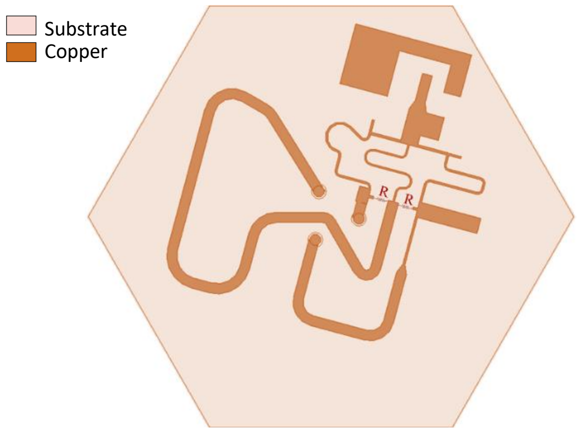

Fig. 13: The designed feeding network.

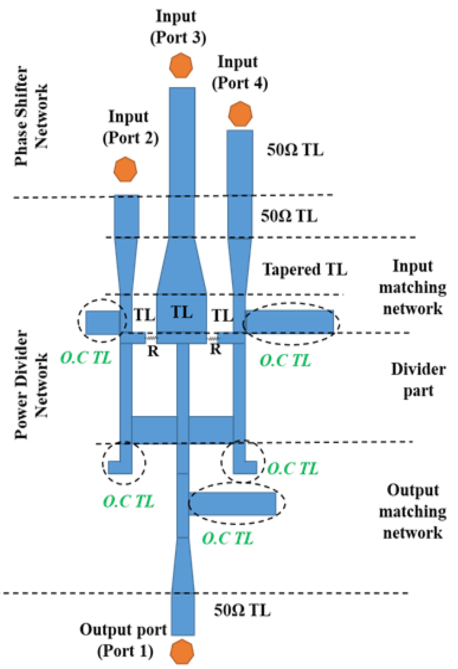

Fig. 14: Schematic of the feeding network elements.

Results and Discussion

The performance of the proposed antenna is evaluated via numerical simulation at CST Studio Suite software. To validate the results, the simulation is repeated in two other software, HFSS and FEKO. The results of the three simulations are depicted in terms of return loss, RHCP, and LHCP radiation pattern in Fig. 15 and Fig. 16, respectively. It is clear that all simulations are in good agreement and this validates the current study.

Fig. 15 shows the S_{11} versus frequency for the proposed antenna. As clearly shown, the simulated antenna is capable to operate at desirable frequency bands, (GPS L1, GLONASS G2, GALILEO E1, and E2), with a bandwidth of 56 MHz (1.558-1.614 GHz).

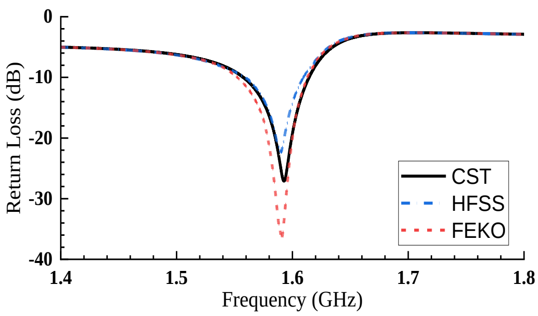

Fig. 15: Return loss.

The RHCP and LHCP radiation patterns of the designed antenna are illustrated in Fig. 16. Results show the RHCP beamwidth of 103°. It is also clear that the FBR of the proposed antenna is 40 dB. Furthermore, on the upper half plane, low LHCP gain is observed. The RHCP gain is 3.45 dB.

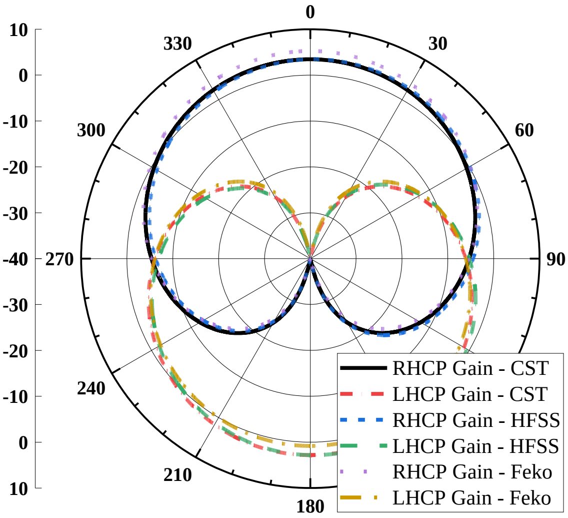

Fig. 16: RHCP and LHCP radiation pattern.

Fig. 17 demonstrates the AR beamwidth and the ratio of right-to-left radiation (R/L). It is clear that below 3 dB AR beamwidth is 108°. Also, in the range of 134°, R/L ratio has a value above 10,

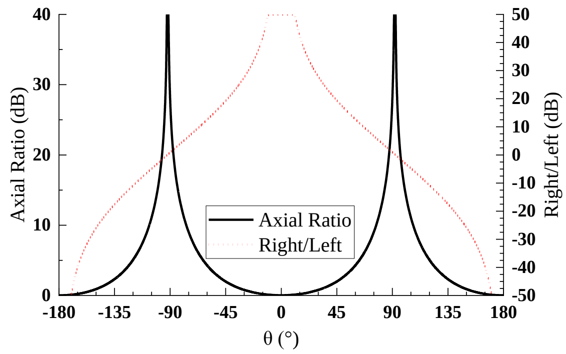

Fig. 17. Axial Ratio and R/L ratio versus theta at the resonant frequency.

The current distribution on the patch layer at the resonant frequency is shown in Fig. 18. Currents are depicted in three consecutive phases of 60°, 120°, and 180°. The current travels in a counter-clockwise direction with successive phase changes. This proves the circular polarization radiation of the proposed antenna.

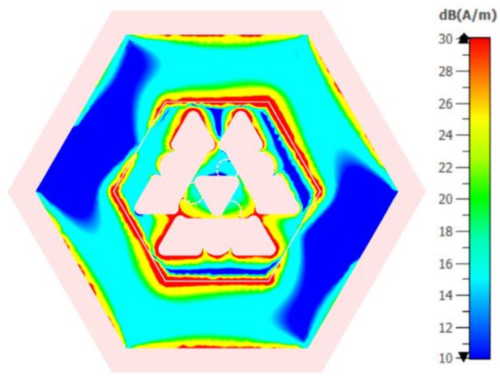

(a)

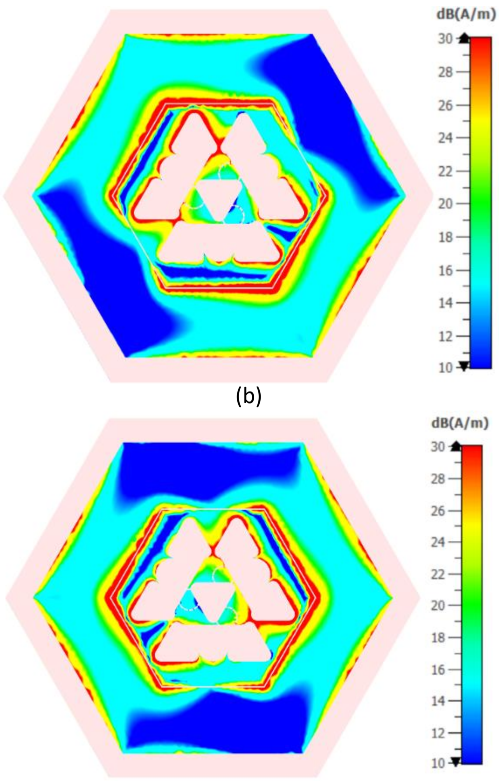

(c)

Fig. 18: Current distribution at different phase shifts; (a) 0° (b) 60° (c) 120°.

Phase stability is considered an important performance parameter for GPS antennas. To achieve phase stability, the antenna phase center variation (PCV) should tend to zero in an ideal case. In Fig. 19, coordinates of the phase center and also PCV for the proposed antenna are displayed towards frequency. As clearly depicted, at the whole antenna operation frequency (1.558-1.614 GHz), the PCV is less than 0.16mm.

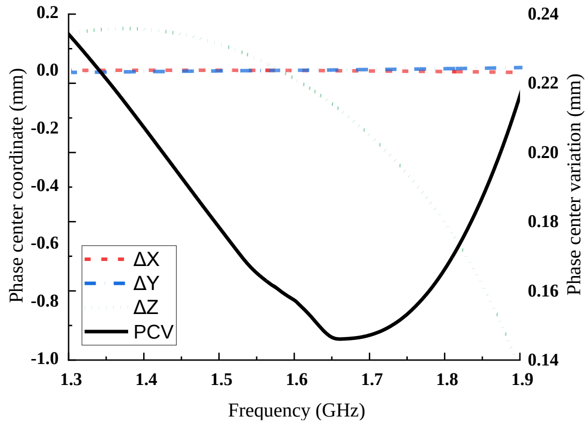

Fig. 19: Phase center coordinate and variation versus operating frequency.

Table 2: Comparison between the proposed antenna and previous studies.

Reference	Substrate	Resonant frequency (GHz)	Antenna area (mm²)	Antenna height (mm)	FBR (dB)	RHCP beamwidth (deg)	Phase center variation (mm)	AR beamwidth (deg)
[1]	FR4	1.575	18496	24.2	25	85	1.2	134
[3]	FR4, Ceramic	1.575	900	4.8	20	83	NS*	153
[27]	organic magnetic substrate	1.575	3600	4	35	90	NS	NS
[30]	Rogers RT/Duroid 5880	1.575	19600	1.6	12	62	NS	NS
[31]	Taconic ORCER Cεr – 10	1.575	10000	3.2	26.22	100	NS	100
[32]	FR4	1.575	3969	1.6	2.7	97	NS	101
[33]	RO3003C	1.575,2.45	5320	3.1	NS	98	NS	121
Proposed antenna	Taconic RF-43	1.575	1756	2	40	103	0.365	108

* Not Stated

▭: Best item

Conclusion

A novel miniaturized, low-cost, multiple-feed, circularly polarized microstrip antenna has been designed for GPS/GLONASS applications. The antenna can operate at GPS L1 (1575 MHz), GLONASS G1 (1602 MHz), Galileo E1 (1589 MHz), and E2 (1561 MHz) bands. For CP radiation, multiple feeds with the coupled technique are used. To miniaturize the antenna, semi-fractal geometry and also novel design of a feeding network are employed. Key features of the proposed antenna are its compact size, high FBR, wide RHCP beamwidth, desirable bandwidth, and AR beamwidth.

The designed antenna size is below 18 cm^2. Numerical simulation results show the proposed antenna has favorable AR of below 3 dB and back-ward radiation below -50 dB with FBR over 40 dB. Additionally, the proposed antenna has bandwidth of 56 MHz (1558-1614 MHz) and a wide RHCP beamwidth of 103°. Furthermore, the PCV is less than 0.16 mm.

Author Contributions

Each part of this paper was contributed by all three authers.

Acknowledgment

The authers would like to thank the reviewers and editor of the JECEI for their valuable comments.

Conflict of Interest

The authors declare no potential conflict of interest regarding the publication of this work. In addition, the ethical issues including plagiarism, informed consent, misconduct, data fabrication and, or falsification, double publication and, or submission, and redundancy have been completely witnessed by the authors.

Abbreviations

CP	Circular Polarization
RHCP	Right Hand Circular Polarization
LHCP	Left Hand Circular Polarization
AR	Axial Ratio
FBR	Front to Back Ratio
PCV	Phase Center Variation

References

[1] F. Bilotti , C. Vegni, "Design of high-performing microstrip receiving gps antennas with multiple feeds," IEEE antennas wirel. Propag. Lett., 9: 248–251, 2010.

[2] Y. M. Cai, K. Li, y. Yin, L. Zhao, "A multi-functional tri-mode patch antenna supporting dual-band gps and wireless communication system," microw. Opt. Technol. Lett., 59: 2457–2462, 2017.

[3] S. J. Jeong, "Compact circularly polarized antenna with a capacitive feed for gps/glonass applications," etri j., 34: 767–770, 2012.

[4] K. A. Yinusa, "A dual-band conformal antenna for gnss applications in small cylindrical structures, " IEEE antennas wirel. Propag. Lett., 17: 1056–1059, 2018.

[5] Nasimuddin, Z. Ning Chen, X. Qing, "Dual-band circularly polarized s-shaped slotted patch antenna with a small frequency-ratio," IEEE trans. Antennas propag., 58: 2112–2115, 2010.

[6] M. A. S. M. Al-haddad, N. Jamel, A. N. Nordin, "Flexible antenna: a review of design, materials, fabrication, and applications," j. Phys. Conf. Ser., 1878: 012068, 2021.

[7] K. A. Yinusa, E. P. Marcos, S. Caizzone, "Robust satellite navigation by means of a spherical cap conformal antenna array," in Proc. 2018 18th International Symposium on Antenna Technology and Applied Electromagnetics (ANTEM), 2018.

[8] E. K. Kaivanto, M. Berg, E. Salonen, P. De maagt, "Wearable circularly polarized antenna for personal satellite communication and navigation," IEEE trans. Antennas propag., 59(12): 4490–4496, 2011.

[9] S. Komeylian, M. Tayarani, S. Hassan, "Design of a novel four-feed dual-band microstrip antenna with pure circular polarization and analysis of circular polarization parameters," int. J. Nonlinear anal. Appl., 14 , 2023.

[10] S. Komeylian, M. Tayarani, S. Hassan, "A novel blind adaptive algorithm applied to new designed smart antenna array for interference suppression," int. J. Nonlinear anal. Appl., 14, 2023.

[11] K. Y. Lam, K. Luk, K. F. Lee, H. Wong, k. B. Ng, "Small circularly polarized u-slot wideband patch antenna," IEEE antennas wirel. Propag. Lett., 10: 87–90, 2011.

[12] Z. Ma, J. Chen, P. Chen, Y. F. Jiang, "Design of planar microstrip ultrawideband circularly polarized antenna loaded by annular-ring slot," int. J. Antennas propag., 2021: 1–10, 2021.

[13] X. Tang, H. Wong, Y. Long, Q. Xue, K. L. Lau, "Circularly polarized shorted patch antenna on high permittivity substrate with wideband," IEEE trans. Antennas propag., 60: 1588–1592, 2012.

[14] S. A. Rezaeieh, "Dual band dual sense circularly polarised monopole antenna for gps and wlan applications," electron. Lett., 47: 1212, 2011.

[15] X. sun, Z. Zhang, Z. Feng, "Dual-band circularly polarized stacked annular-ring patch antenna for gps application," IEEE antennas wirel. Propag. Lett., 10: 49–52, 2011.

[16] N. K. Suyan, F. Lal lohar, C. Dhote, Y. Solunke, "Design of circularly polarized irnss receiver antenna using characteristic mode analysis, " proc. Conecct 2020 - 6th IEEE int. Conf. Electron. Comput. Commun. Technol., pp. 3–7, 2020.

[17] J. Sze, W. Chen, "Axial-ratio-bandwidth enhancement of a microstrip-line-fed circularly polarized annular-ring slot antenna," IEEE trans. Antennas propag., 59: 2450–2456, 2011.

[18] C. Lin, F.-S. Zhang, Y.-C. Jiao, f. Zhang, x. Xue, "a three-fed microstrip antenna for wideband circular polarization," IEEE antennas wirel. Propag. Lett., 9: 359–362, 2010.

[19] Y. M. Cai, K. Li, Y. Z. Yin, X. Ren, "Dual-band circularly polarized antenna combining slot and microstrip modes for gps with his ground plane," IEEE antennas wirel. Propag. Lett., 14: 1129–1132, 2015.

[20] S. Gao, Q. Luo, F. Zhu, circularly polarized antennas. Chichester, uk: john wiley & sons, ltd, 2014.

[21] S. Komeylian, S. Komeylian, F. H. Kashani, "Anisotropic uniaxial crystal as a substrate in spherical microstrip antenna with annular-circular patch and air gap layer," 2014 int. Work. Antenna technol. Small antennas, nov. Em struct. Mater. Appl. Iwat: 385–388, 2014.

[22] S. M. Kim, K. S. Yoon, W. G. Yang, "Dual-band circular polarization square patch antenna for gps and dmb," Microw. Opt. Technol. Lett., 49: 2925–2926, 2007.

[23] G. Byun, H. Choo, S. Kim, "Design of a small arc-shaped antenna array with high isolation for applications of controlled reception pattern antennas," IEEE trans. Antennas propag., 64: 1542–1546, 2016.

[24] H. Chen, Y. Wang, Y. Lin, C. Lin, s. Pan, "Microstrip-fed circularly polarized square-ring patch antenna for gps applications, "IEEE trans. Antennas propag., 57: 1264–1267, 2009.

[25] S. Komeylian, S. Komeylian, "Deploying an ofdm physical layer security with high rate data for 5g wireless networks," IEEE canadian Conference on Electrical and Computer Engineering (CCECE), 2020: 1–7, 2020.

[26] S. Shrestha, S. R. Lee, D. Y. Choi, "A new fractal-based miniaturized dual band patch antenna for rf energy harvesting," int. J. Antennas propag., 2014: 1–9, 2014.

[27] E. Wang, Q. Liu, "gps patch antenna loaded with fractal ebg structure using organic magnetic substrate," prog. Electromagn. Res. Lett., 58: 23–28, 2016.

[28] H. Malekpoor, M. Shahraki, "Compact broadband microstrip triangular antennas fed by folded triangular patch for wireless applications," adv. Electromagn., 10: 14–23, 2021.

[29] M. Moore, Z. Iqbal, S. Lim, "A size-reduced, broadband, bidirectional, circularly polarized antenna for potential application in wlan, wimax, 4g, and 5g frequency bands," prog. Electromagn. Res. C, 114: 1–11, 2021.

[30] A. R. Alajmi, M. A. Saed, "A pin-loaded microstrip patch antenna with the ability to suppress surface wave excitation," prog. Electromagn. Res. C, 62: 131–137, 2016.

[31] K. K. So, H. Wong, K. M. Luk, C. H. Chan, "Miniaturized circularly polarized patch antenna with low back radiation for gps satellite communications," IEEE trans. Antennas propag., 63: 5934–5938, 2015.

[32] Z. Mar Phyo, T. May Nway, K. Kyu Kyu Win, H. Myo Tun, "Development of microstrip patch antenna design for gps in myanmar," am. J. Electromagn. Appl., 8: 1, 2020.

[33] Y. A. Sheikh, K. N. Paracha, S. Ahmad, A. R. Bhatti, A. D. Butt, S. K. A. Rahim, "Analysis of compact dual-band metamaterial-based patch antenna design for wearable application," arab. J. Sci. Eng., 47: 3509–3518, 2022.

Biographies

Saeed Komeylian was born in Tehran, Iran, in 1989.He received the B.Sc. degree from the IKIU, Qazvin, Iran, in 2011, the M.Sc. degree from Sharif University of Technology, Tehran, Iran in 2013, and he is a PhD student in the Faculty of Electrical Engineering, IUST, Tehran, Iran.

- Email: Komeylian.official@gmail.com
- ORCID: 0000-0001-6367-1985
- Web of Science Researcher ID: NA
- Scopus Author ID: NA
- Homepage: NA

Majid Tayarani was born in Tehran, Iran, in 1962.He received the B.Sc. degree from the University of Science and Technology, Tehran, Iran, in 1988, the M.Sc. degree from Sharif University of Technology, Tehran, Iran in 1992, and the Ph.D. degree in communication and systems from the University of Electro-Communications, Tokyo, Japan, in 2001. From 1990 to 1992, he was a Researcher with the Iran Telecommunication Center, where he was involved with nonlinear microwave circuits. Since1992, he has been a member of the faculty with the Department of Electrical Engineering, Iran University of Science and Technology, Tehran, Iran, where he is currently an Associate Professor. His research interests are qualitative methods in engineering electromagnetic, electromagnetic compatibility (EMC) theory, computation and measurement techniques, microwave and millimeter-wave linear and nonlinear circuit design, microwave measurement techniques, and noise analysis in microwave signal sources.

- Email: m_tayarani@iust.ac.ir
- ORCID:0000-0001-8605-0428
- Web of Science Researcher ID:
- Scopus Author ID
- Home pgae: http://ee.iust.ac.ir/content/13094/Dr.Tayarani

Seyed Hassan Sedighy was born in Qaen, South Khorasan, Iran, in 1983. He received his B.Sc., M.Sc. and Ph.D. degrees all in Electrical Engineering from Iran University of Science and Technology (IUST), in 2006, 2008 and 2013, respectively. From December 2011 to July 2012, he was with the University of California, Irvine as a Visiting Scholar. He joined the School of New Technologies at IUST, as an Assistant Professor in 2013.

- Email: sedighy@iust.ac.ir
- ORCID: 0000-0002-5813-5616
- Web of Science Researcher ID:
- Scopus Author ID
- Home page: http://www.iust.ac.ir/page.php?slct_pg_id=13647&sid=94&slc_lang=en

How to cite this paper:
S. Komeylian, M. Tayarani, S. H. Sedighy, "Design of miniaturized microstrip antenna with semi-fractal structure for GPS/GLONASS/Galileo applications," J. Electr. Comput. Eng. Innovations, 11(2): 373-382, 2023.

DOI: 10.22061/jecei.2023.9352.609

URL: https://jecei.sru.ac.ir/article_1843.html